 FDMP, vol.1, no.2, pp.153-169, 2005

How Does Buoyancy-driven Convection Affect Biological Macromolecular Crystallization? An Analysis of Microgravity and Hypergravity Effects by Means of Magnetic Field Gradients

N.I. Wakayama[1], D.C. Yin[2] and J.W. Qi[3]

Abstract: The production of crystals of adequate size and high quality is the "bottleneck" for three-dimensional structure analysis of protein crystals. In this work, in order to shed additional light on the (still controversial) beneficial effect of microgravity on crystal growth, we focus on recent advanced experimental and theoretical research about the effects of buoyancy-driven convection on protein crystallization. In the light of the numerical studies the following major outcomes can be highlighted: (1) when the crystal size exceeds several dozens of μm, buoyancy-driven convection dominates solute transport near the growing crystal and the crystal growth rate becomes larger than that under zero gravity. (2) The ratio of the side-surface growth rate to the top-surface growth rate increases with crystal size because of convection and the ratio is about three when the crystal size is 100 μm. The ratio of the side-surface growth rate to the top-surface growth rate measured experimentally confirms these results (the averaged value for 127 protein crystals was determined to be about two). Thus, both numerical and experimental studies provide a solid basis to the idea that convection strongly affects the crystal growth rate. Moreover, since according to experiments about the dependence of crystal quality on effective gravity (hypergravity or microgravity obtained by means of magnetic field gradients), protein crystals (e.g., orthorhombic lysozyme or snake muscle fructose-1,6-bisphosphatase) exhibit better quality with decreasing the gravity level, buoyancy-driven convection may be thought of as also affecting crystal quality in a detrimental way.

keyword: Convection, crystal growth, crystal growth rate, crystal quality, gravity, microgravity, protein crystal.

[1] National Institute for Materials Science, Tsukuba, Ibaraki, 305-0003, Japan
Email: wakayama.nobuko@nims.go.jp
[2] Northwestern Polytechnical University, Xian 710072, Shaanxi, P.R. China
[3] University of Maryland, College Park, Maryland 20742, USA

1 Introduction

Proteins are the elementary building units of living creatures, and the molecular structure of proteins provides the basis for understanding the functions of biological macromolecules and enables further evolutionary progress in biomaterials and biotechnology applications, including new therapeutic drugs, insecticides, herbicides, efficient industrial enzymes etc. Determining the structure of protein molecules is therefore crucial. The most powerful technique for determining macromolecular structure is X-ray crystallography. Along these lines, developments in beam technology, detectors, and computational crystallography have greatly accelerated the determination of these structures. However, the production of crystals of adequate size and high quality is often the "bottleneck" for three-dimensional structure analysis of protein crystals.

The crystallization of protein molecules is an empirical science of rational trial and error guided by previous studies (McPherson, 1999). The development of general methods to improve crystal quality is essential. The term "protein crystal growth" is often historically used to describe the macromolecular crystallization experiments. Here, the terms protein or macromolecule are used to refer to many varied biological molecules, including viruses, proteins, DNA, RNA etc. Protein crystal growth can be regarded as a multi-parametric process whose evolution is influenced by a variety of physical, chemical and biological parameters. As one of the most important parameters affecting protein crystal growth, we consider gravity. Crystallization experiments conducted in space have indicated that about 20% of crystals grown in space yield better X-ray diffraction data than the best crystals grown on Earth (Kundrot, Judge, Pusey and Snell, 2001). An obvious difference between

space- and Earth-based experiments is the reduction of buoyancy-driven convection and crystal sedimentation. In order to understand why microgravity is beneficial for growing high quality crystals, it is necessary to understand how gravitational field affects protein crystal growth.

The growth of a protein crystal from an aqueous solution is coupled to solute convection around the crystal. As shown in Fig. 1, when a crystal grows from a solution, the recruitment of solute from the surrounding solution produces a steep concentration gradient near the crystal. Since the concentration near the crystal C_l is less than that of the bulk solution C_∞ ($C_l < C_\infty$), buoyancy-driven convection occurs around the crystal. The Rayleigh number for solute convection during protein crystal growth can be defined as $Ra_{solute} = g\left(\Delta\rho/\rho\right)L^3/\nu D$, where $\Delta\rho$ is the density difference, ρ is the bulk solution density, L is the depth of solution and D is the protein molecule diffusion coefficient. Assuming typical values, i.e. $D = 7\times10^{-11}m^2/s$, $\Delta\rho/\rho = 0.01$, $\nu = 10^{-6}m^2/s$, and L=0.01m, Ra_{solute} is 1.4×10^{10}. On the other hand, the Rayleigh number for thermal convection in water is defined as $Ra_{thermal} = g\beta_T\Delta TL^3/\nu\alpha$, where β_T is the thermal expansion coefficient, α is the thermal conductivity and ΔT is the temperature difference. For typical values $\nu = 10^{-6}m^2/s$, $L = 0.01m$, $\beta_T = 2.5\times10^{-4}K^{-1}$, ΔT=1K and $\alpha = 1.457\times10^{-7}m^2/s$, $Ra_{thermal}$ is 1.68×10^4.

Thus, Ra for solute convection is extraordinary large compared with Ra for thermal convection. Therefore, buoyancy-driven convection may be thought of as significantly affecting the process of protein crystal growth and crystal quality. However, the effects of buoyant-convection on protein crystal growth remain controversial in the literature. In this review paper, theoretical and experimental research focusing on buoyancy-driven convection effects is described.

First, we summarize some interesting numerical studies about the effects of buoyancy-driven convection on protein crystal growth (Section 2); then, experimental studies about the effect of buoyancy-driven convection on crystal growth rates using magnetic orientation are discussed in Section 3. In 1996, a new method to control effective gravity using a vertical magnetic force was proposed (Wakayama 1996; Wakayama, Ataka and Abe, 1997). This method is described in Section 4. Using this technique, the dependence of crystal quality on effective gravity was investigated from microgravity conditions to 1.8 g (Section 5) and from 0.7 g to 1.3 g (Section 6). Finally, we discuss the methods to yield high quality protein crystals.

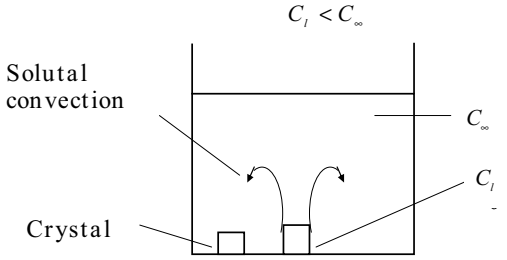

Figure 1 : Solute convection occurs near the protein crystal when the crystal is segregated from the aqueous solution.

2 Numerical study about the effects of buoyancy-driven convection on protein crystal growth

In order to clarify how gravitational field affects the various transitional stages of protein crystal growth, we consider solute convection near specimens growing from microcrystals suspended in solution as well as large crystals sedimented at the bottom (crystal size: 0.1-100 μm) (Qi and Wakayama, 2000). For comparison, we also consider crystal growth under zero gravity condition.

2.1 Theoretical model

As shown in Fig. 2, we assume a cylindrical crystal $2R$ in diameter and $2R$ in height, growing from protein solutions in a cylindrical container 5 mm in diameter and 5 mm high. Two crystal positions are assumed: when the crystal size is less than 4 μm, the crystal is assumed to be suspended in the center of the container, and when the size is above 10 μm, the crystal is assumed to be sedimented to and located at the bottom of the container. The flow is assumed to be two dimensional and axisymmetric. The growth velocity is sufficiently low that a fixed boundary can be regarded as a reliable approximation.

Therefore, the size of a growing crystal is assumed to be constant. The top surface of the solution is treated as a free surface. For other walls and the crystal surface, no-slip flow conditions are imposed. The boundary conditions imposed on the concentration field are $C = C_l$ at the

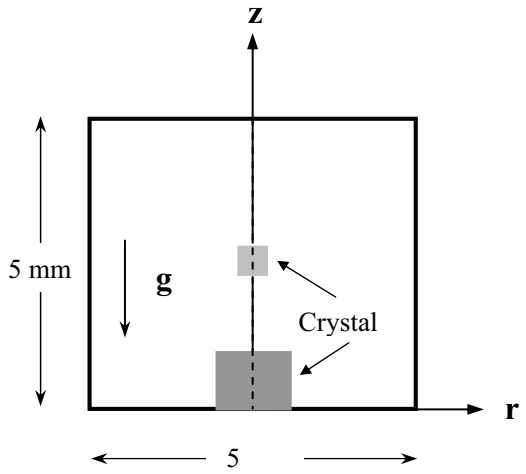

Figure 2 : Model geometry.

crystal interface, $C = C_\infty$ at the container side-walls, and $\nabla C \cdot \mathbf{n}$ =0 on the symmetry axis and the other container walls, where $\mathbf{n}$ is the unit vector normal to the boundary surface. The density difference of the solution is approximately proportional to the difference in the protein concentration. Therefore, the density of the solution (ρ) can be expressed as a linear function of the protein concentration:

$$\rho \approx \rho_l \left[1 + \left(\frac{\rho_\infty - \rho_l}{\rho_l}\right)\left(\frac{C - C_l}{C_\infty - C_l}\right)\right] = \rho_l\,(1 + \Gamma_S \phi) \quad (1)$$

where C is the solute concentration in solution, $\phi = (C - C_l)/(C_\infty - C_l)$ is the dimensionless concentration, and $\Gamma_S = (\rho_\infty - \rho_l)/\rho_l$. As anticipated, the subscripts l and ∞ represent the crystal interface and a position far from the crystal, respectively.

The value for C_l is somewhere between the saturation concentration and the supersaturation, C_∞. In general, C_l is dependent on the growth system and generally not known for most protein crystal growth systems. For simplification, C_l is assumed to be constant.

The governing equations for flow and solute concentration are as follows:

Equation of continuity:

$$\nabla \cdot \left(\rho \vec{\mathbf{V}}\right) = 0 \quad (2)$$

Equation of motion:

$$\rho \frac{\partial \vec{V}}{\partial t} + \vec{V} \cdot \nabla(\rho \vec{V}) = \rho \vec{g} - \nabla p + \rho \nu \nabla^2 \vec{V} \quad (3)$$

Equation of dimensionless concentration:

$$\partial \phi / \partial t + \vec{V} \cdot \nabla \phi = D_S \nabla^2 \phi \quad (4)$$

where $\vec{V}$,p, t, and $\mathbf{g}$ are the velocity vector, pressure, time, and gravitational acceleration vector, respectively. Other physical properties are: D_s (the diffusion coefficient) = 7×10^{-11}m^2/s, ν (kinematic viscosity)=10^{-6}m^2/s, and Γ_s= 0.00795 (lysozyme).

2.2 Numerical method

The governing equations, Eqs. (2) to (4), together with the initial and boundary conditions were solved by using a finite volume method and the SIMPLEC algorithm (Van Doormaal and Raithby, 1984) to handle the coupling between velocity and pressure. In practice, the density is assumed to be constant in Eqs. (2-3) except insofar as it gives rise to a gravitational force. The approximation is extremely accurate for many flows, and makes the mathematics and physics simpler.

A 102×52 non-uniform grid was used in the simulations. A finer grid was used near the crystal interface to achieve high resolution of the velocity and concentration fields near the solution-crystal interface, where the gradients are large.

2.3 Results and discussions

2.3.1 Convection and concentration fields for growing crystal suspended in solution

In the initial stage of crystallization, microcrystals grow suspended in the solution after nucleation and most of them settle to the bottom when their size is in the range 2-6 μm (Ataka, Katoh and Wakayama, 1997; Wakayama, 1998). First, we present simulations of the flow and concentration fields for growing crystals suspended in solution. Figs. 3 (a) and (b) shows flow and concentration fields in the vicinity of the growing crystal the size of which is 1 and 4 μm in diameter, respectively. There is a well-known convective flow pattern with a rising plume near the crystal. When the crystal size is 1 μm, the maximum buoyancy driven velocity, about 1.45 μm/s, occurs

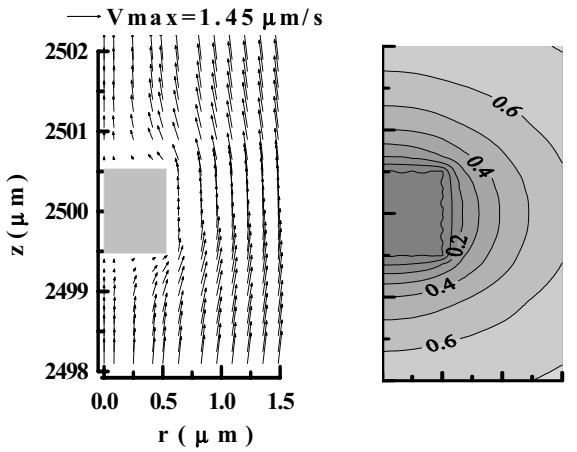

(a) 1 μm, 1g

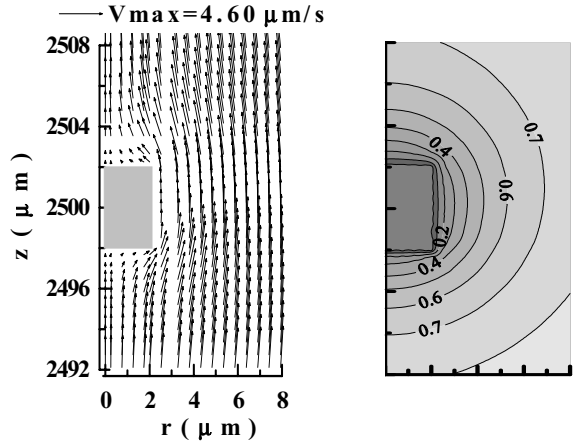

(b) 4 μm, 1g

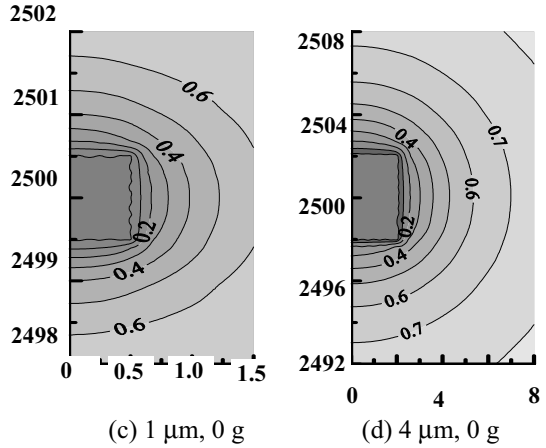

(c) 1 μm, 0 g (d) 4 μm, 0 g

Figure 3 : Flow (left) and concentration fields (right) near suspended crystals in solution (steady state) under normal gravity conditions for crystals the size of which are (a) 1, (b) 4μm. Concentration fields under zero gravity conditions for crystals the size of which are (c) 1, (d) 4 μ m.

in the plume above the growing crystal. Figs. 3 (c) and (d) show concentration fields near growing crystals under zero gravity condition. As shown in Fig. 3(a) and (c), when the crystal size is 1 μm, the concentration distribution near the crystal surface is not significantly affected by buoyancy-driven flow and concentration distribution under normal gravity is similar to that under zero gravity condition. When the crystal size is 4 μm, the maximum velocities, V_{max} is 4.60 μm/s. As shown in Fig. 3, with increasing crystal size from 1 to 4μm, buoyancy-driven flow is enhanced and slightly alters the purely diffusive concentration distribution that occurs under zero gravity.

2.3.2 *Convection and concentration fields for growing crystal at the bottom of a container*

Most crystals settle to the bottom when they grow above several micrometers. Fig. 4 shows flow (left) and concentration fields (right) in the vicinity of 10, 50, and 100 μm crystals growing at the bottom of the container. The maximum buoyancy-driven velocity is always observed in the plume above the growing crystal and V_{max} increases from 9.78 to 62.7 μm/s with increasing the crystal size from 10 to 100 μm. Furthermore, in comparison with growth under zero gravity condition (Fig. 5), the concentration field near the crystal surface is greatly distorted by buoyancy-driven convection when the size exceeds several dozens of μm.

Fig. 6 shows the distribution of dimensionless concentration (ϕ) along the radial axis at the crystal half-height ($z=z_0$) under normal gravity and zero gravity.

A solid line indicates the distribution under zero gravity. The deviation of the distribution from diffusion controlled growth (0g) increases with increasing crystal size, and in zero gravity, there exists a relatively large zone depleted in protein in contact with the crystal surface. Thus, these results indicate that under normal gravity condition, solute transport is typically dominated by buoyancy-driven convection when the crystal grows above several dozens of microns.

2.3.3 *Dependence of crystal growth rate on interfacial solute concentration gradient*

According to a mass balance and to Fick's first law, the local crystal growth rate, V, at the crystal surface can be expressed as (Grant and Saville, 1991):

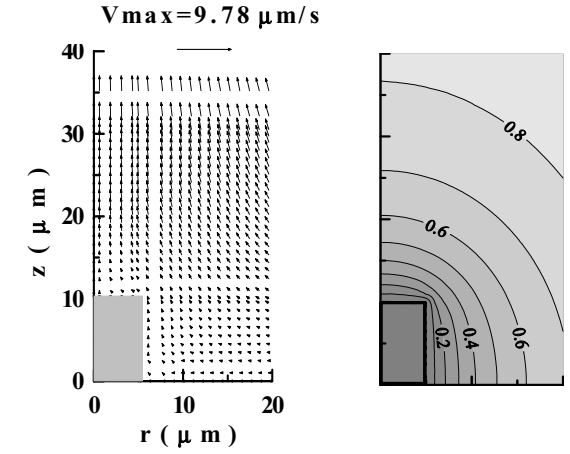

(a) 1 0 μm

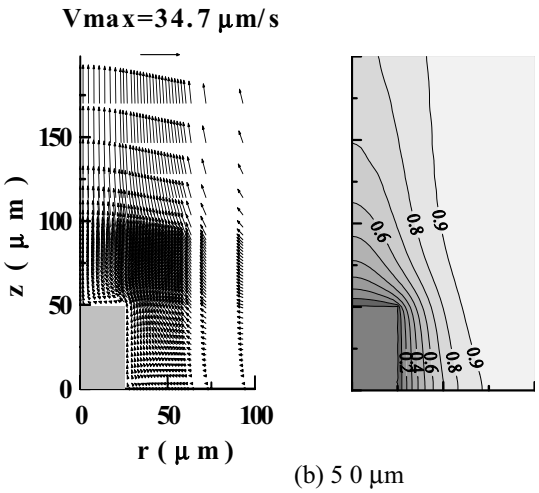

(b) 5 0 μm

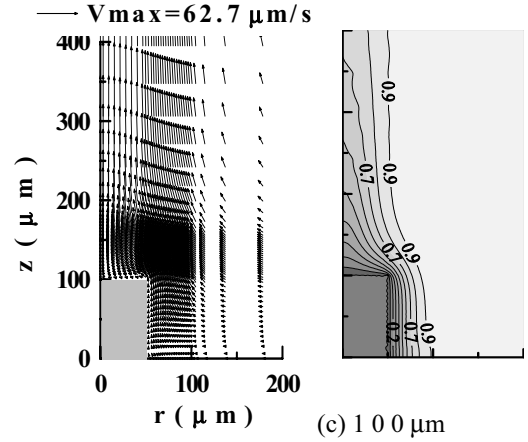

(c) 1 0 0 μm

Figure 4 : Flow (left) and concentration fields (right) in the vicinity of sedimented crystals at the bottom of the container in normal gravity (steady state). Crystal sizes of (a) 10, (b) 50, and (c) 100 μ m.

$$V = \frac{D_S}{C_X}\frac{\partial_C}{\partial_n} = \frac{D_S\,(C_\infty - C_l)}{C_X L}\frac{\partial\phi}{\partial\overline{n}} \tag{5}$$

where C_X is the mass concentration of solute in the crystal, L is the height of the cylindrical container, and $\overline{n} = n/L$ is a dimensionless coordinate normal to the crystal surface. According to Eq. (5), V depends on the concentration difference between the solution far from the crystal interface and the interface $(C_\infty - C_l)$, and the local dimensionless concentration gradient at the crystal surface,$\partial\phi/\partial\overline{n}$.

Fig. 7 shows the distribution of concentration gradient, $\partial\phi/\partial\overline{n}$ along the top (a) and side surfaces (b) of crystals growing at the bottom of a container. Under both normal and zero gravity conditions, $\partial\phi/\partial\overline{n}$, i.e., crystal growth rates decrease with increasing crystal size. Compared with crystal growth in zero gravity, buoyancy-driven convection promotes crystal interfacial growth because the concentration gradients at the top and side surfaces (-o-) in normal gravity are higher than those in zero gravity condition (–). This difference increases with increasing crystal size.

As shown in Fig. 8, the ratio of the side-surface growth rate to the top-surface growth rate in normal gravity increases with crystal size. For example, when the crystal size is 100μm, the side-surface growth rate is about three times that of the top-surface. Such difference in growth rate caused by buoyant convection will affect the crystal habit.

Fig. 9 shows the relationship between crystal size and $\partial\phi/\partial\overline{n}$ at the half height of the side of the crystal interface (r=R, z=z_o), under normal and zero gravity conditions. With increasing crystal size, $\partial\phi/\partial\overline{n}$ decreases under both normal and zero gravity conditions. These results could explain why it is difficult to obtain large crystals. Furthermore, the effect of convection on $\partial\phi/\partial\overline{n}$ appears when the crystal size is about 10 μm, increases with increasing crystal size and becomes dominant above several dozens of μm. This indicates that the most volume of the crystal is formed under the condition where the buoyancy dominates solute transport near the crystal. For example, if the crystal size is 100μm, 99.9% of the volume is thought to grow under the effects of buoyant convection. Therefore, it is important to damp buoyancy-driven convection in order to produce high quality crystals.

The major outcomes of the numerical study are:

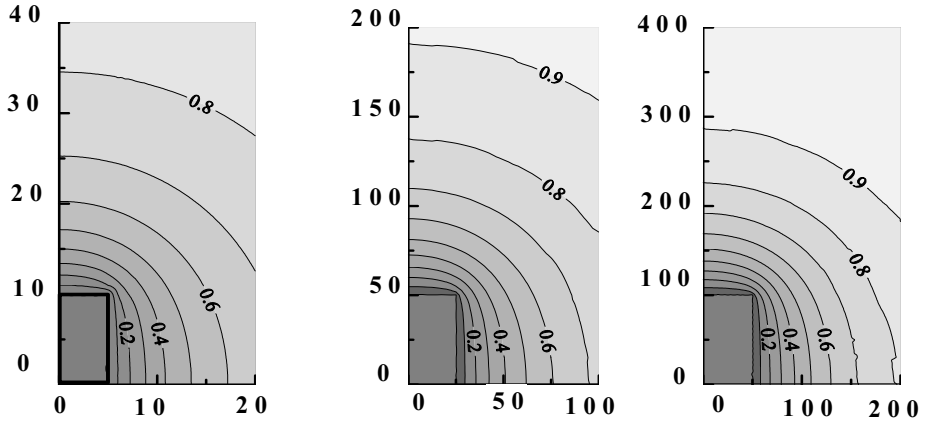

(a) 10 μm (b) 50 μm (c) 100 μm

Figure 5 : Concentration fields in the vicinity of crystals at the bottom of a container under zero gravity condition (steady state).

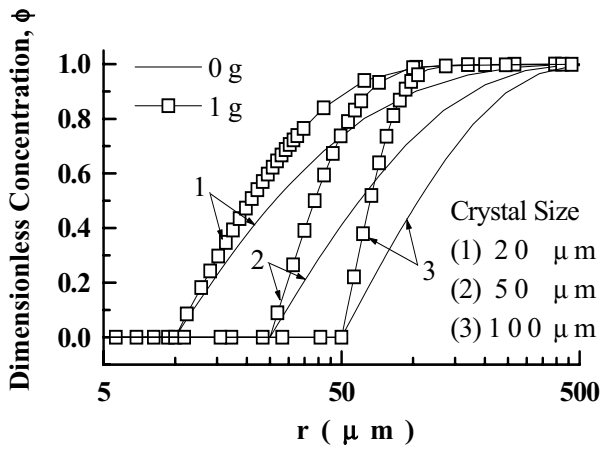

Figure 6 : Distributions of dimensionless concentration (ϕ) along the radial axis at the crystal half height ($z=z_o$).

(1) When the size of growing crystals exceeds several dozens of μm, buoyancy-driven convection dominates solute transport near the growing crystals. The contribution of buoyancy-driven convection to crystal growth rate increases with crystal size.

(2) The ratio of the side-surface growth rate to the top-surface growth rate in normal gravity conditions increases with increasing crystal size. Such difference in growth rates will affect the crystal habit.

3 Experimental study to determine the ratio of the side-surface growth rate to the top-surface growth rate

When the crystal size is 100μm, the side-surface growth rate is calculated to be about three times that of the top-surface as shown in Fig. 8. In order to provide a solid basis to these results, the ratio of the side-surface growth rate to the top-surface growth rate was measured using 127 crystals by Yin, Wakayama, Wada and Huang (2003).

3.1 Experimental procedure

The orthorhombic crystal ($P2_12_12_1$, with a=79.0, b=80.8 and c=37.5 Å) (Yin, Oda, Wakayama and Ataka, 2003) was grown using paramagnetic $NiCl_2$as the crystallization agent. Magnetic orientation was used as a tool to align the c-axis of the crystal in either horizontal direction or vertical direction (Worcester, 1978; Ataka, Katoh and Wakayama, 1997; Wakayama, 1998). A supersaturated solution was prepared by mixing an equal volume of the lysozyme aqueous solution (80 mg/*ml*) and $NiCl_2$ solution (160 mg/ *ml*). The pH was 4.60. The crystallization was carried out batchwise in a glass vessel (ϕ18mm$\times$50mm), and the solution height in the vessel was kept at about 10mm. The vessel was set inside a copper water jacket to keep the temperature at 21˚C by flowing temperature-controlled water through the jacket. Crystals were grown for two days in the ab-

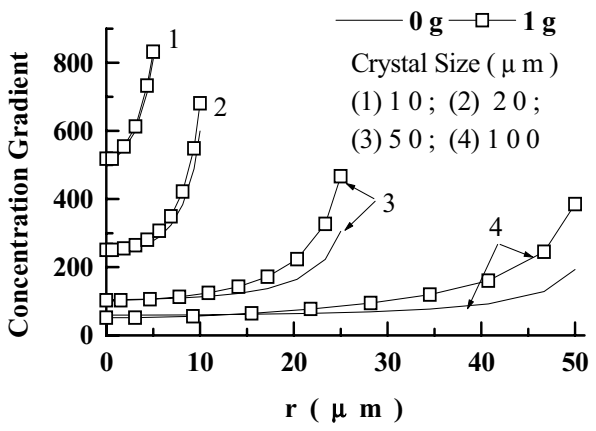

(a) Top surface

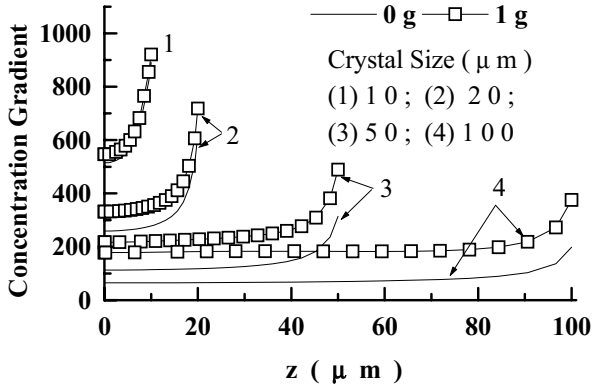

(b) Side surface

Figure 7 : Distributions of dimensionless concentration gradient ($\partial\phi/\partial\overline{n}$) at (a) the top and (b) side surfaces of crystals sedimented at the bottom of the container under zero gravity and normal gravity conditions.

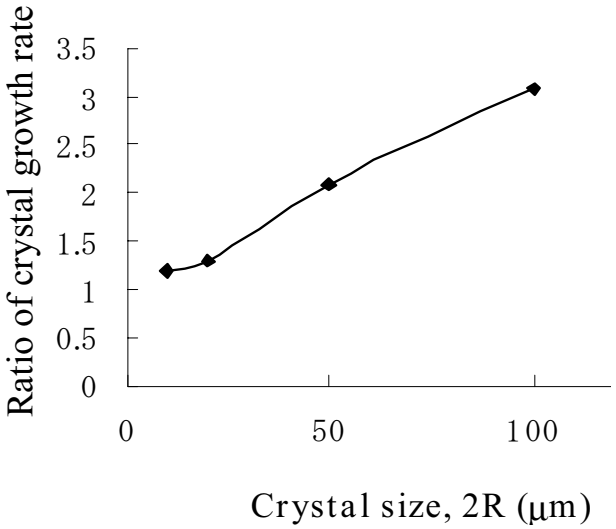

Figure 8 : Relationship between crystal size (2R) and the ratio of the side-surface growth rate to the top-surface growth rate in normal gravity.

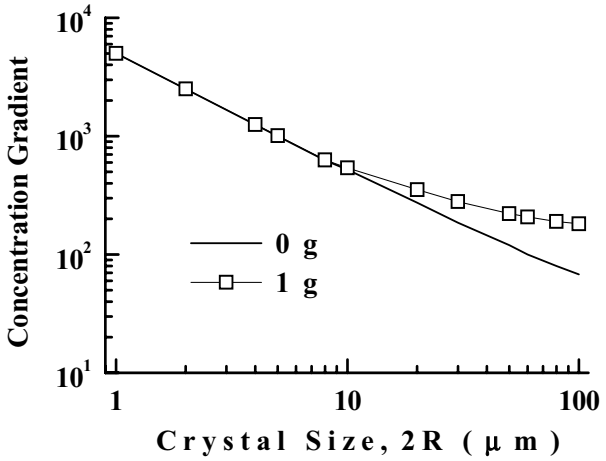

Figure 9 : Effect of crystal size (2R) on the dimensionless concentration gradient ($\partial\phi/\partial\overline{n}$) at the half height of the side of the crystal interface (r=R, z=z_o).

sence and presence of a 10 T uniform magnetic field generated by a superconducting magnet (JMTD-10T100M, Japan Superconductor Technology Inc.). The direction of a magnetic field, which was parallel to the central axis of solenoid coil of the superconducting magnet, was kept horizontally or vertically.

3.2 Results and discussion

3.2.1 Orthorhombic lysozyme crystals in the presence and absence of a magnetic field

Figures 10(a)-(d) show photographs of orthorhombic lysozyme crystals crystallized by $NiCl_2$ in the absence and presence of 10 T uniform magnetic field. In the absence of the field [Figs. 10(a) and (b)], crystals exhibit

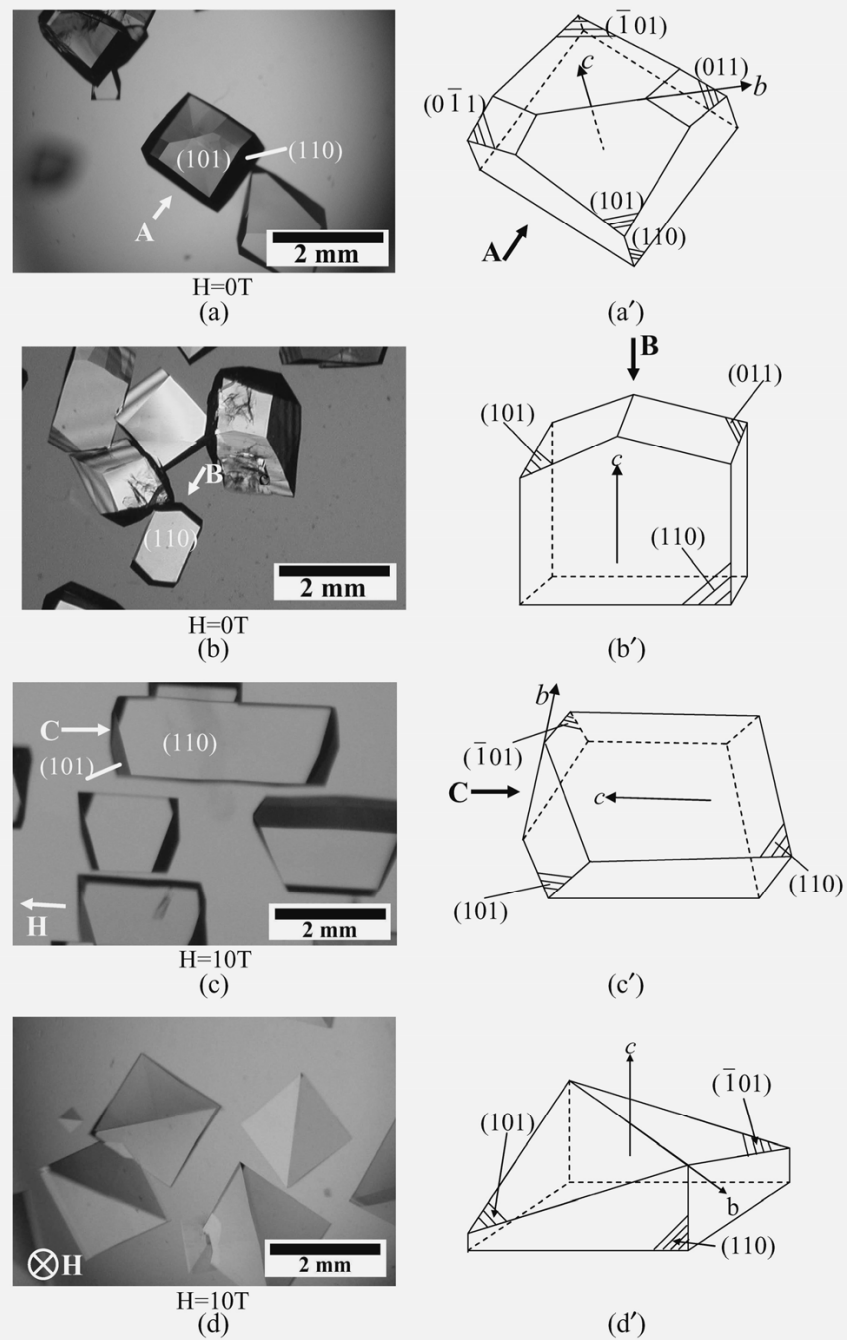

Figure 10 : Habit of orthorhombic lysozyme crystals grown using $NiCl_2$ as crystallization agent (a, b) in the absence of a magnetic field, (c) in the presence of a horizontal magnetic field (10T), (d) in the presence of a vertical magnetic field (10T). (a′-d′) Miller indices of the crystallographic faces. Vector **H** indicates the direction of the magnetic field.

various morphologies, and the directions of their crystal axes are random. In the presence of the horizontal magnetic field [Fig. 10(c)], however, the crystals show more uniform morphology and all of them are aligned with their *c*-axes along the horizontal magnetic field. The crystals grown in the vertical magnetic field show much more uniform morphology [Fig. 10(d)], namely, typical roof-like crystals reported previously (Yin, Oda, Wakayama, Ataka, 2003), and their *c*-axes are oriented along the direction of the vertical magnetic field. Thus,

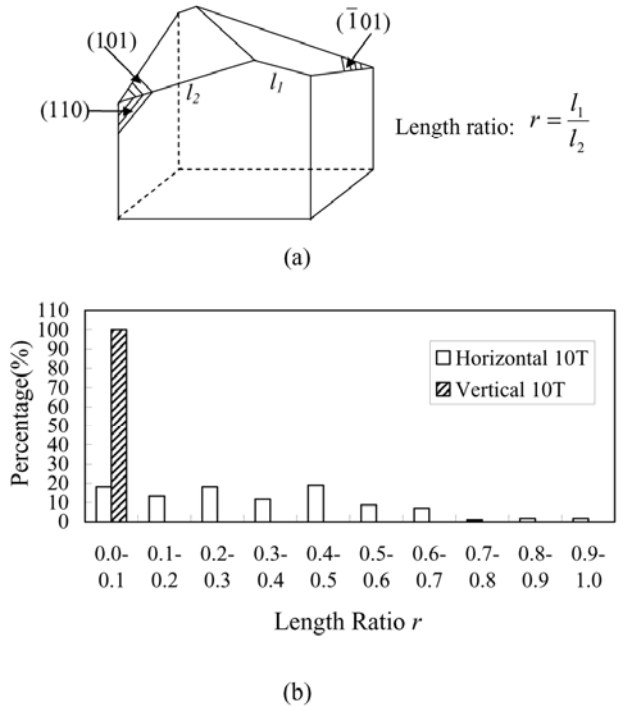

Figure 11 : Distribution of length ratio r of the crystals grown in the presence of a vertical (n=33, n: the total number of crystals for data collection) and horizontal magnetic field (n=127). Length ratio r is defined as the ratio of the shorter length l_1 to longer length l_2 of the edge lines between the {110} faces and {101} faces.

crystals grown in the absence of a magnetic field show diverse morphologies, whereas crystals grown in the presence of either a horizontal or vertical magnetic field of 10 T are featured by a more uniform morphology.

According to X-ray diffraction analysis (Yin, Oda, Wakayama, Ataka, 2003), the lattice constants of roof-like crystals are similar to those of tetragonal crystals ($a = b$ = 79.20 Å, c = 37.94 Å) (Datta, Biswal and Vijayan, 2001), and the coordination of a Ni^{2+} ion to Asp52Oδ2 atom in a lysozyme molecule distorts the normal tetragonal lattice into an orthorhombic lattice.

3.2.2 *Effects of magnetic orientation on crystal morphology*

Although roof-like crystals, *i.e.*, crystals with only two opposite {101} faces, appear when grown in the presence of either a horizontal or vertical magnetic field, the crystals grown in a vertical magnetic field [Fig. 10(d)], show a much more uniform habit than those grown in a horizontal field [Fig. 10(c)]. To quantify the diversity in habit, we chose the length ratio of the edge lines between the {101} and {110} faces as a parameter for comparison. As shown in Fig. 11(a), this length ratio r can be defined as the ratio of the smaller length l_1 to larger l_2 length, so that r is always less than 1. The distribution of r for our experimental results is given in Fig. 11(b). The habit of the crystals grown in the vertical magnetic field is uniform and their r concentrates at around ~ 0, whereas in the presence of the horizontal field, r is spread over the range of $0 \sim 0.7$.

Next, we introduce some theoretical arguments to illustrate how this difference in the r distribution is correlated with the growth rates of {110} and {1$\bar{1}$0} faces when the crystals are the roof-like type. According to the numerical simulation in Section 2, the ratio of the side-surface growth rate to the top-surface growth rate increases with crystal size. For example, when the crystal size is 100 μm, the ratio is calculated to be about three (see Figs. 7 and 8).

Fig. 12 shows crystal growth in vertical (a) and horizontal magnetic fields (b). When crystals are grown in a vertical magnetic field [Fig. 12(a)], all of the four {110} and {1$\bar{1}$0} faces are vertical. When the growth rate of the (110) and ($\bar{1}\bar{1}$0) faces, V_1, is faster than that of the ($\bar{1}$10) and (1$\bar{1}$0) faces, V_2, a roof-like morphology will not appear [Figs. 12(a-i)]. Only when $V_1 = V_2$, will a roof-like morphology appear [Fig. 12(a-ii)]. Therefore, the experimental result that all of the crystals appear "roof-like" indicates that the vertical four faces have the same growth rate.

On the other hand, in a horizontal magnetic field [Fig. 12(b)], the initial size and shape of the roof-like crystals (or nuclei) grown are assumed the same as those grown in a vertical magnetic field [Fig. 12(a)]. Because the mass transport conditions near the top and two side surfaces differ from each other, their growth rates might be affected by buoyancy-driven convection. We assume that the (110) and ($\bar{1}\bar{1}$0) faces perpendicular to the bottom of the vessel have the same growth rate, V_1, while the growth rate of the (1$\bar{1}$0) face facing upward is assumed to be V_2[Fig. 12(b)].

The habit of the crystals depends on the difference in growth rates V_1 and V_2. When $V_1 > V_2$, the habit shown in Fig. 12(b-i) appears. In our experiments, when the field was applied horizontally, such habit was frequently observed [see Fig. 10(c)] (r= 0.1∼0.7; about 80% of the

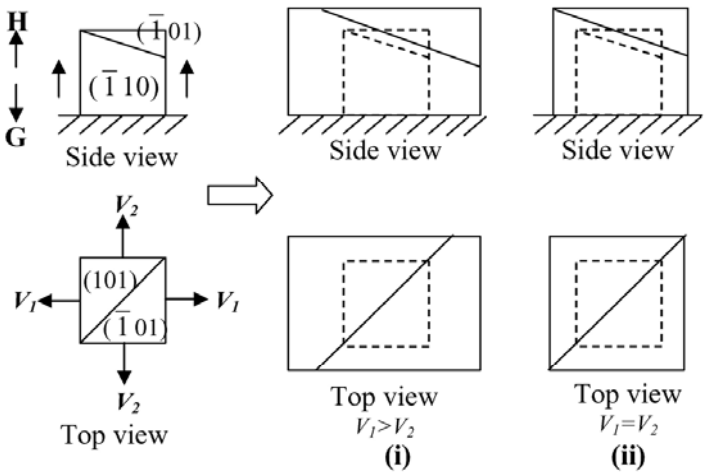

(a)

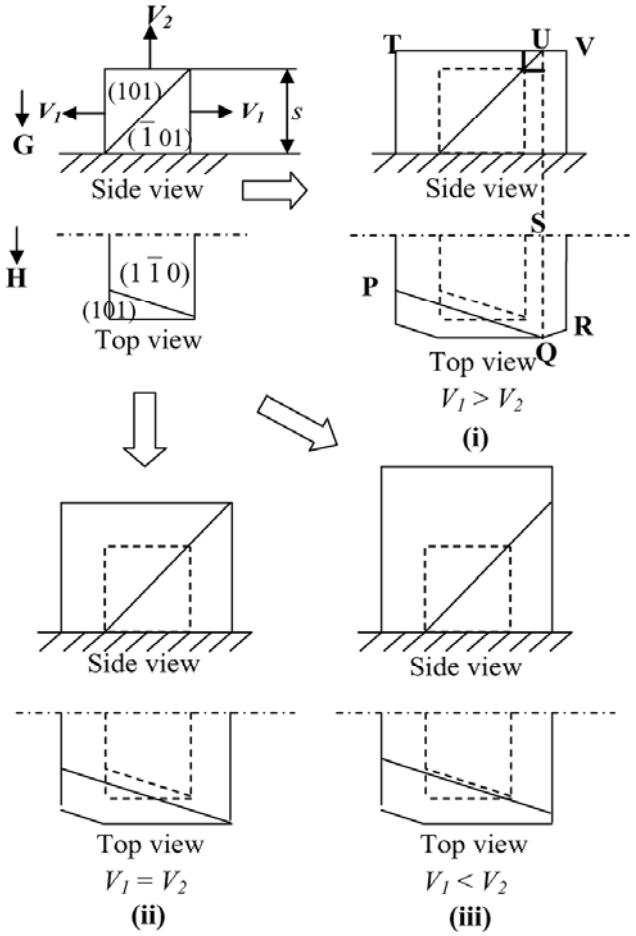

(b)

Figure 12 : Schematic of the finally grown crystal habit as a function of growth rates of $\{110\}$ and $\{1\bar{1}0\}$ faces, V_1 and V_2, respectively, in the presence of a (a) vertical and (b) horizontal magnetic field.

total number of the crystals appeared like this in Fig. 11), indicating that the faces perpendicular to the vessel bottom had larger growth rates than those of the faces facing upward. This observation agrees well with the numerical simulation that the growth rate of a side surface is larger than that of the top surface (Sec. 2). When $V_1 = V_2$, the habit in Figure 12(b-ii) appears. We also observed such habit experimentally like in Fig. 10(c) (r= 0∼0.1; about 18% of the total number of the crystals appeared like this in Fig. 11). When $V_1 < V_2$, the habit [Fig. 12(b-iii)] will appear. However, we did not observe such habit experimentally. These results indicate that the orientation of the crystals causes differences in the growth environments of $\{110\}$ and $\{1\bar{1}0\}$ faces by buoyancy-driven convection, resulting in differences in the growth rates of $\{110\}$ faces, thus yielding various habits.

3.2.3 *Relationship between the length ratio (r) and the growth rate ratio (V_2/V_1) of the {110} and {1$\bar{1}$0} faces*

Here, we discuss the relationship between r and V_2/V_1 in order to explain the microscopic appearance of crystals grown under a vertical or horizontal magnetic field. If we assume that the starting crystal is a nucleus, *i.e.*, $s \approx 0$ [where s is the side length of the seed crystal; Fig. 12(b)] and that the two faces of "roofs" grow at the same rate, then the relationship between r and V_2/V_1 can be estimated.

In Fig. 12(b), the growth rate of the top face and the two side vertical faces are V_2 and V_1, respectively, and r is defined as QR/PQ. Because ∠SQR=∠SQP, UV/QR=TU/PQ,

$$r = QR/PQ = UV/TU = \frac{V_1 t - V_2 t}{s + V_1 t + V_2 t} \tag{6}$$

where t is the growth time.

If s = 0, then Eq. (6) becomes

$$\frac{V_2}{V_1} = \frac{1-r}{1+r}. \tag{7}$$

According to the distribution of r in Fig. 11(b) together with Eq. (7), in a vertical magnetic field, r = 0, and thus $V_2 = V_1$. In a horizontal magnetic field, V_2/V_1 of 127 crystals ranges between 1 ∼ 0.2 (r ranged between 0 ∼ 0.7) and the averaged $\{V_2/V_1\}$ is 0.54. Thus, V_2/V_1can be determined from the experiment. This result proves that buoyancy-driven convection significantly affects the process of protein crystal growth.

Our simulation was conducted assuming one crystal though in the experiments, many crystals were grown in the vessel. Recently, Lappa et al. studied numerically and experimentally the growth of protein crystals when many crystals grew at the same time and showed that the effects of buoyancy convection can become even more complex when the crystals are sufficiently close and mutual interaction occurs (Lappa, 2003, 2005; Lappa, Piccolo and Carotenuto, 2003).

The major outcomes of the experimental study can be summarized as follows:

(1) Magnetic orientation by applying a horizontal magnetic field causes differences in the growth environments of $\{110\}$ and $\{1\bar{1}0\}$ faces of orthorhombic lysozyme crystals due to buoyancy-driven convection, resulting in differences in growth rates and thus different crystal morphologies.

(2) It is determined that the side-surface growth rate is twice the top surface growth rate. This result agrees with the numerical results in Section 2.

4 Method to control effective gravity from microgravity to hypergravity on Earth

4.1 Principle to control effective gravity

For a long time, there have been few methods to efficiently damp natural convection in electrically low-conducting fluids such as protein aqueous solutions on Earth. The cost of space experiments is expensive and the opportunities for experiments are limited. However, recently, a new method to control effective gravity was proposed (Wakayama, 1996; Wakayama, Ataka and Abe, 1997; Brooks, Reavis, Medwood, Stalcup, Meisel, Steinberg, Arnowitz, Stover, and Perenboom, 2000; Wakayama, Zhong, Kiyoshi, Itoh and Wada, 2001). In a space platform, a microgravity environment is generated because gravitational force is balanced by centrifugal force. A newly developed method to control effective gravity uses a vertical magnetic (Kelvin) force instead of centrifugal force,and it is applicable to the control of buoyancy-driven convection in electrically low- and non-conducting fluids (Huang and Gray, 1998; Qi, Wakayama and Ataka, 2001; Qi and Wakayama, 2004). Fig. 13

shows the principle to control effective gravity. The vertical force acting on water in a container is equal to the difference between the gravitational force, F_g and an applied magnetic force, F_m. Hence, the effective gravity acting on water can be tuned from 0g to 1g by simply changing the magnitude of an upward magnetic force, F_m.

A magnetic (Kelvin) force which is a body force is proportional to density and acts on every material even if it is not ferromagnetic. Generally, a unit volume of a substance in a 1D magnetic field gradient experiences a force F_m(McGraw-Hill Encyclopedia of Science and Technology, 1992) given by:

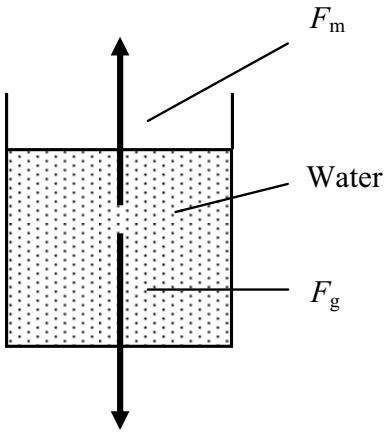

Figure 13 : Principle to control effective gravity.

$$F_m = \mu_0 \chi H \left(dH/dy\right) = \rho \mu_0 \chi_g H \left(dH/dy\right) \tag{8}$$

where μ_0 is the absolute magnetic permeability of vacuum, y the site coordinate and χ the magnetic susceptibility per unit volume, χ_g the magnetic susceptibility per unit weight, and ρghe density.

Most materials, such as water and many proteins, are diamagnetic, and experience a weak repulsive force along the steepest gradient of the magnetic field strength because χ_g<0. On the other hand, an attractive force acts on paramagnetic materials and ferromagnetic materials (iron etc.). Because F_m is proportional to material density (as shown by Eq. (8)), its superposition on gravity can partially reduce or enhance effective gravity (vertical acceleration). When a vertical force, F_m is applied along the gravitational force F_g, the total force acting on a fluid is

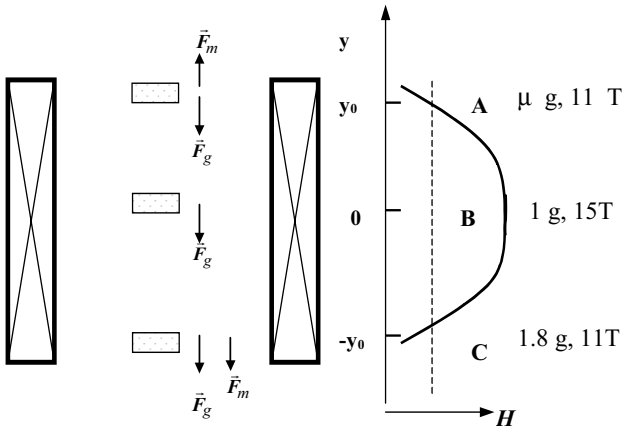

Figure 14 : Schematics of how to control effective gravity. Figure (b) shows the spatial distribution of the magnetic field strength of a superconducting magnet (LH15T40, JASTEC). A: Microgravity, B: Normal gravity, C: Hypergravity.

$$F = F_g \pm F_m = \rho \left\{ g \pm \left| \mu_0 \chi_g H \left(dH/dy\right) \right| \right\} = \rho qg,$$
$$q = 1 \pm \left| \left(\mu_0 \chi_g / g\right) H \left(dH/dy\right) \right| \tag{9}$$

This equation indicates that, in practice, the level of effective gravity q can be modified continuously by changing the value of $H(dH/dy)$. When $\mu_0^2 H \left(dH/dy\right)$ = -1370 T^2/m and an upward F_m corresponding to $F_m/\rho g$=1 acts on pure water (χ_g =-9.0×10^{-9}m^3·kg^{-1}), we may expect to produce a microgravity environment.

4.2 Superconducting magnet to generate microgravity for long duration

For protein crystal growth, generating microgravity environment over a period of days or weeks is crucial. Until recently, a large magnetic field gradient of $\mu_0^2 H \left(dH/dy\right)$ =-1370 T^2/m could be produced for only several hours by a massive hybrid-magnet. Since 2002, however, a convenient type of superconducting magnet (LH15T40, Japan Superconductor Technology Inc.) can generate a magnetic field gradient of -1370 T^2/m for more than several weeks, thanks to its persistent current

mode system (Hirose, Saito, Watanabe and Tanimoto, 2002). Fig. 14(a) shows the cross-section schematic of a vertical superconducting magnet, and Fig. 14(b) shows the spatial distribution of the magnetic field strength H along a vertical central y-axis for the magnet (LH15T40). When $\mu_0^2 H\left(dH/dy\right)$ =-1370 T^2/m at position **A**, an upward F_m corresponding to ρg acts on pure water (χ_g =-9.0×10^{-9}m$^3\cdot$kg^{-1}), thus a microgravity environment is expected.

On the other hand, when $\mu_0^2 H\left(dH/dy\right)$ =1100 T^2/m at position **C**, a downward F_m corresponding to $0.8\rho g$ is established, and a hypergravity environment of 1.8 g is expected. At the center of the magnet (position **B**) where field strength is 15T and its gradient is 0 T^2/m, F_m is zero and the gravity level is 1g.

5 Formation of protein crystals (orthorhombic lysozyme) in various effective gravity (μ g-1.8 g)

5.1 Experimental procedure

Protein crystal formation experiments were conducted for the first time using the newly developed superconducting magnet (LH15T40) by Yin, Wakayama, Harata, Fujiwara, Kiyoshi, Wada, Niimura, Arai, Huang, and Tanimoto (2004). Orthorhombic lysozyme crystals were grown at 40.0±0.1˚C by the conventional batch method. The final concentration of the solution was 60mg/*ml* lysozyme and 40mg/ *ml* NaCl. The pH was 4.60. Immediately after the supersaturated solution was prepared, it was separately injected into small vessels which were placed both inside and outside the magnet. As shown in Fig. 14(a) and (b), three positions were used (**A**: μg/11T, **B**: 1g/15T, **C**: 1.8g/11T) inside the magnet. Simultaneously, samples were also placed outside the magnet (1g/0T) as controls. The size of the vessels was ϕ6.5 mm×16.5 mm. Solution volume in each vessel was 100 μL and the solution height was about 3 mm. The duration of the crystallization was two days. After crystallization, the best looking crystals of similar size were chosen from different positions for analysis.

There are several parameters that indicate the quality of protein crystals: the signal to noise ratio of diffracted intensity (I/σ), overall B-factor, mosaicity, the R_{merge} value, rocking curve, and the maximum resolution etc. Because most parameters are significantly affected by crystal volume, it is difficult to compare the quality of one crystal to another. Here, the crystal quality was compared using the overall B-factor, because it is essentially independent of crystal volume.

The overall B-factor was obtained in the following way: X-ray diffraction data were measured on a Bruker SMART6000 diffractometer with CuKα radiation from a MAC Science MX06 rotating anode generator. The data sets were processed with the programs SaintPlus (Bruker) and Madnes (Nonius). An overall B-factor, as well as a scale factor, was calculated by the equation:

$$Y = \left\{ I_{obs}(hkl) \Big/ \sum_i f_j^2 \right\} = k \cdot \exp\left(-2B \cdot \sin^2\theta/\lambda^2\right) \quad (10)$$

Eq.(10) indicates the relationship between the experimental data $I_{obs}(hkl)$, the apparent temperature factor B and the scale factor k. Y is the intensity, which is normalized by the atomic form factor f_j and λ is the wavelength (1.5418 Å). To determine B and k, the equation can be rewritten in the following form:

$$\ln(Y) = \ln(k) - 2B\frac{\sin^2\theta}{\lambda^2} \quad (11)$$

Wilson plot can then be drawn by plotting [ln(Y)] vs. $\left(\sin\theta/\lambda\right)^2$. If the B-factor is low, the slope of the Wilson plot will be close to linear in the high angle range. It indicates that high-resolution diffraction spots can be observed. Therefore, we can assume that a low B-factor corresponds to a good-quality crystal.

5.2 Experimental results and discussions

Fig. 15 shows the results of three experiments, using the overall B-factor. The numbers in circles and triangles represent the number of experimental runs.

(1) Comparison between microgravity-grown crystals and 1.8g grown crystals:

The magnetic field strength (11T) at microgravity position (**A**) is the same as that at 1.8 g (**C**) [see Fig. 14(b)]. Therefore, the comparison of crystals formed in microgravity and hypergravity makes it possible to examine purely the dependence of effective gravity on crystal quality. Generally the overall B-factor is not very sensitive to crystal quality because thermal vibration mostly contributes to this factor. However, as shown in Fig. 15, in the three sets of experimental results, the overall B-factors of the crystals obtained at μg are always smaller

than those of the crystals obtained at 1.8 g. Since lower B-factor indicates better quality, the quality of crystals obtained at μg is always better than those at 1.8 g. This result provides experimental evidence for the fact that the difference in crystal quality comes from the difference in effective gravity, i.e. buoyancy-driven convection.

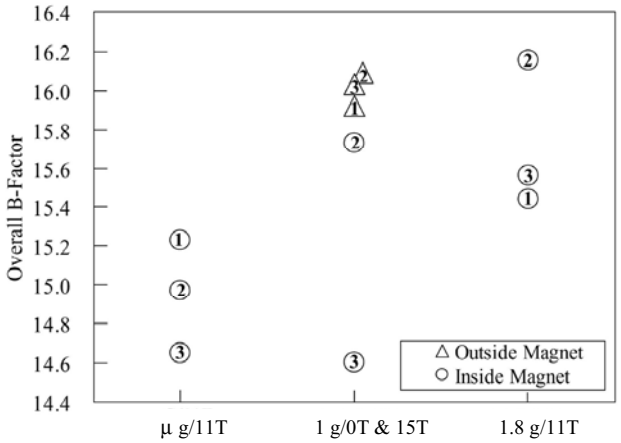

Figure 15 : Quality comparisons of orthorhombic lysozyme crystals obtained at effective microgravity, normal gravity and hypergravity inside a superconducting magnet and normal gravity outside the magnet. The numbers in the circles and triangles represent the number of different experimental runs.

In microgravity, buoyancy-driven convection is effectively damped, while it is promoted at hypergravity. In Sections 2 and 3, we have discussed theoretical and experimental research about the effects of buoyancy-driven convection on the crystal growth rate. The present result clearly demonstrates that buoyancy-driven convection deteriorates crystal quality. The same tendency was also observed for crystals of snake muscle fluctose-1,6-bisphosphatase (Lin, Zhou, Azzi, Xu, Wakayama and Ataka, 2000).

(2) 1g-grown crystals in the presence and absence of magnetic field (15 T):

At the center of the magnet [position **B** in Fig. 14(a)], field strength is 15T and the gravity level is the same as outside,*i.e.*, 1g. Therefore, comparing the crystal quality formed at position **B** with that outside the magnet, we can examine purely the effect of magnetic field per se on the crystal quality. As shown in Fig. 15, the crystals obtained inside the magnet (15T) show better quality than those obtained outside. This result agrees with the previous results on orthorhombic lysozyme crystals (Sato, Yamada, Saijo, Hori, Hirose, Tanaka, Sazaki, Nakajima, Igarashi, Tanaka and Matsuura, 2000). On the other hand, for snake muscle fluctose-1,6-bisphosphatase (Lin, Zhou, Azzi, Xu, Wakayama and Ataka, 2000), the placing the sample at the center of a magnet (10T) did not clearly improve the crystal quality.

Recently, the effects of strong magnetic fields on protein crystal quality have been studied by Sato et al. (2000), Ataka and Wakayama (2002) and Wakayama (2003). Currently, four mechanisms are known [see Table 2 in ref. (Wakayama, 2003)], and all of them may contribute to the improvement of crystal quality. Low-gravity environment is obtained by applying a magnetic field gradient, while other mechanisms such as magnetic orientation of crystals, damping of natural convection by Lorentz force *etc*. work in both uniform and gradient magnetic fields. Thus, a strong magnetic field seems to improve crystal quality rather than to deteriorate it.

The major outcomes are:

(1) Orthorhombic lysozyme crystals show better quality with decreasing effective gravity from 1.8 g to μg.

(2) Both microgravity and magnetic field itself contribute to the improvement in crystal quality of orthorhombic lysozyme.

6 Formation of protein crystals (snake muscle fructose-1,6-bisphosphatase) under various effective gravity (0.7-1.3 g)

Interesting protein crystal formation experiments were conducted under various effective gravity conditions ranging from 0.7 to 1.3g by Lin, Zhou, Azzi, Xu, Wakayama and Ataka (2000). The protein used was snake muscle fructose-1,6-bisphosphatase (MW=36000), which is a series of enzymes that controls the sugar level in blood. At present, details of the molecular structure of this protein have not been determined.

6.1 Experimental apparatus and procedures

The protein crystal formation experiments used a commercially available liquid-helium free superconducting magnet (JMTD-10T100M, JASTEC). Crystals were grown simultaneously at three positions (**A**: 0.7 g/7 T, **B**: 1g/10T, **C**: 1.3 g/7 T) inside the magnet [see Fig. 14(a)]. Simultaneously, samples were also placed out-

side the magnet (1g/0T) for controls. The crystal formation experiments were conducted four times. Crystals were grown by batch crystallization. For crystals grown in each position, an X-ray oscillation photograph of a crystal of similar size was taken for comparison. The resolution shell whose signal-to-noise ratio was 2 was used as an indicator of crystal quality.

6.2 Results and discussion

Fig. 16 shows the results. The resolution of the crystals formed in 0.7-0.8 g was about 3.06±0.14 Å, whereas that of crystals formed outside the magnet (o) was 4.24 ±1.24 Å. Thus, the lower gravity improved the resolution of crystals by about 30%. When crystals were grown inside the magnet (Δ), the crystal showed better quality with decreasing effective gravity from 1.3 to 0.7 g.

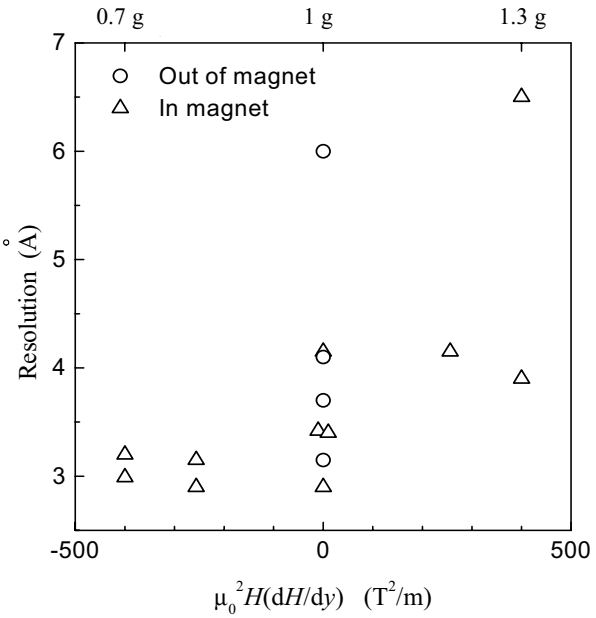

Figure 16 : Resolution of protein crystals (snake muscle fructose-1,6-bisphosphatase) as a function of effective gravity (0.7-1.3g). Experimental results are summarized in Table 1 in ref. (Lin, S. X. et al., 2000).

This tendency is an additional demonstration for the fact that the level of effective gravity is an important factor in determining crystal quality and buoyancy-driven convection deteriorates crystal quality.

The key points of the present study are:

(1) Crystals of snake muscle fructose-1,6-bisphosphatase shows better quality with decreasing effective gravity from 1.3 g to 0.7 g.

(2) This tendency suggests again that buoyancy-driven convection deteriorates crystal quality

7 Concluding remarks

This review summarizes some recent numerical and experimental research about the effects of buoyancy-driven convection on protein crystal growth. The conclusions can be summarized as follows:

(1) According to the numerical simulations, the contribution of buoyancy-driven convection to protein crystal growth increases with crystal size. When the crystal size exceeds several dozens of microns, convection dominates solute transport near the growing crystals.

(2) According to the numerical simulations, the ratio of the side-surface growth rate to the top-surface growth rate increases with crystal size because of buoyant-driven convection, and the ratio is about three when the crystal size is $100\mu m$.

(3) The ratio of the side-surface growth rate to the top-surface growth rate of 127 crystals was measured. The averaged value of the ratio was about two, and this result agrees with the numerical result (2).

(4) Orthorhombic lysozyme crystals show better quality with decreasing effective gravity from 1.8 g to μg. Snake muscle fructose of 1,6-bisphosphatase crystals also show the same tendency with decreasing effective gravity from 1.3 g to 0.7 g.

Thus, the theoretical and experimental studies prove that buoyancy-driven convection affects crystal growth rate and crystal quality. Therefore, in order to obtain high quality protein crystals, it is important to damp solute convection. Empirically, scientists know how to get high quality crystals, and they have grown protein crystals under conditions where buoyant convection is damped, for example, small volume of protein solution, crystallization in gel phase etc.

Improving the quality of protein crystals is a challenging work. Along these lines, protein crystallization in virtual microgravity generated by a superconducting magnet can be regarded as a very promising strategy. The utilization of a microgravity environment generated by a vibration-free, durable superconducting magnet will provide an environment for growing high quality biological

macromolecular crystals. Furthermore, this means can be also used to get additional insights into the physics of the problem. If we grow crystals under both microgravity and hypergravity and compare the quality of the crystals obtained, we can learn whether microgravity improves crystal quality or not. This kind of tests will allow us to select promising proteins, crystal formation methods and conditions prior to the space experiments. Of course, further experiments with many other proteins are required to test the generality of these approaches.

References

Ataka, M.; Katoh, E.; Wakayama, N. I. (1997): Magnetic orientation as a tool to study the initial stage of crystallization of lysozyme. *J. Cryst. Growth*, vol.173, pp. 592-596.

Ataka, M.; Wakayama, N. I. (2002): Effects of a magnetic field and magnetization force on protein crystal growth. Why does a magnet improve the quality of some crystals?. *Acta Crystallogr.*, vol. D58, pp. 1708-1710.

Brooks, J.S.; Reavis, J.A.; Medwood, R.A.; Stalcup, T.F.; Meisel, M.W.; Steinberg, E.; Arnowitz, L.; Stover, C.C.; Perenboom J.A.A.J. (2000): New opportunities in science, materials, and biological systems in the low-gravity (magnetic levitation) environment. *J. Appl. Phys.,* vol. 87, no. 9, pp. 6194-6199.

Datta, S.; Biswal, B.K.; Vijayan, M. (2001): The effect of stabilizing additives on the structure and hydration of proteins: a study involving tetragonal lysozyme. *Acta Crystallogr.* vol. D 57, no. 11, pp.1614-1620.

Grant, M. L.; Saville, D. A. (1991): The role of transport phenomena in protein crystal-growth. *J. Cryst.Growth,* vol. 108, no.1-2, pp.8-18.

Hirose, R.; Saito, K.; Watanabe, Y.; Tanimoto, Y. (2002): Development of a superconducting magnet for high magnetic force application. *Proceedings of 6th Symposium on New Magneto-Science,* Tsukuba, Japan, Nov. 6-8, pp. 198-199.

Huang, J.; Gray, D. D. (1998): Magnetic control of convection in nonconducting diamagnetic fluids. *Phys. Rev. E,* vol. 58, no. 8, pp.5164-5167.

Kundrot, C.E.; Judge, R.A.; Pusey, M.L.; Snell, E.D. (2001): Microgravity and macromolecular crystallography. *Cryst. Growth Design,* vol. 1, no. 1, pp. 87-99.

Lappa, M. (2003): Growth and mutual interference of protein seeds under reduced gravity conditions. *Phys. Fluids*, vol. 25, no. 4, pp. 1046-1057.

Lappa, M. ; Piccolo, C.; Carotenuto, L. (2003): Numerical and experimental analysis of periodic patterns and sedimentation of lysozyme. *J. Cryst. Growth*, vol. 254, no.3- 4, pp. 469-486.

Lappa, M. (2005): Discrete layers of interacting protein seed: Convective and morphological stages of evolution. *Phys. Rev. E*, vol. 71, no. 031904, Part 1, pp. 1-12.

Lin, S. X.; Zhou, M.; Azzi, A.; Xu, G.; Wakayama, N. I.; Ataka, M. (2000): Magnet used for protein crystallization: novel attempts to improve the crystal quality. *Biochem. Biophys. Res. Commun.,* vol. 275, pp. 274-278.

McPherson, A. (1999): *Crystallization of Biological Macromolecules.* Cold Spring Harbor Laboratory Press.

McGraw-Hill Encyclopedia of Science and Technology (1992; 7th, Edn.); vol.10, p. 315, McGraw-Hill.

Qi, J. W.; Wakayama, N. I. (2000): Solutal convection during the whole process of protein crystal growth. *J. Cryst. Growth,* vol. 219, pp. 465-476.

Qi, J. W.; Wakayama, N. I.; Ataka, M. (2001): Magnetic suppression of convection in protein crystal growth processes. *J. Cryst. Growth*, vol. 232, pp. 132-137.

Qi, J.W.; Wakayama, N. I. (2004): The combined effects of magnetic field and magnetic field gradients on convection in crystal growth. *Phys. Fluids,* vol. 16, no. 9, pp. 3450-3459.

Sato, T.; Yamada, Y.; Saijo, S.; Hori, T.; Hirose, R.; Tanaka, N.; Sazaki, G.; Nakajima, K.; Igarashi, N.; Tanaka, M.; Matsuura, Y. (2000): Enhancement in the perfection of orthorhombic lysozyme crystals grown in a high magnetic field (10 T). *Acta Crystallogr.,* vol. D56, no. 8, pp. 1079-1083.

Van Doormaal, J. P.; Raithby, G. D. (1984): Enhancements of the simple method for predicting incompressible fluid-flows. *Numerical Heat Transfer,* vol. 7, no. 2, pp. 147-163.

Wakayama, N.I. (1996): Control of Effective Gravity, Japan patent 3278685, applied 1996; US patent 6596076.

Wakayama, N. I.; Ataka, M.; Abe, H. (1997): Effect of a magnetic field gradient on the crystallization of hen lysozyme. *J. Cryst. Growth,* vol. 178, pp. 653-656.

Wakayama, N.I. (1998): Quantitative study of crystallization kinetics of hen egg-white lysozyme using mag-

netic orientation: *J. Cryst. Growth,* vol. 191, pp. 199-205.

Wakayama, N. I.; Zhong, C. W.; Kiyoshi, T.; Itoh, K., Wada, H. (2001): Control of vertical acceleration (Effective gravity) between normal- and micro-gravity. *AIChE J.,* vol. 47, pp. 2640-2643.

Wakayama, N.I. (2003): Effects of a strong magnetic field on protein crystal growth. *Cryst. Growth Design,* vol. 3, pp. 17-24.

Worcester, D. L. (1978): Structural origins of diamagnetic anisotropy in proteins. *Proc. Natl. Acad. Sci. USA,* vol. 75, no. 11, pp. 5475-5477.

Yin, D. C.; Wakayama, N. I.; Wada, H.; Huang, W. D. (2003): Significant effects of magnetic and gravitational fields on the morphology of protein crystals (orthorhombic lysozyme crystals grown using $NiCl_2$ as crystallization agent). *J. Phys. Chem. B,* vol. 107, pp. 14140-14144.

Yin, D. C.; Oda, Y.; Wakayama, N. I.; Ataka, M. (2003): New morphology, symmetry, orientation and perfection of lysozyme crystals grown in a magnetic field when paramagnetic salts ($NiCl_2$, $CoCl_2$ and $MnCl_2$) are used as crystallizing agents. *J. Cryst. Growth,* vol. 252, pp. 618-625.

Yin., D. C.; Wakayama, N. I.; Harata, K.; Fujiwara, M.; Kiyoshi, T.; Wada, H.; Niimura, N.; Arai, S.; Huang, W. D.; Tanimoto, Y. (2004): Formation of protein crystals (orthorhombic lysozyme) in quasi-microgravity environment obtained by superconducting magnet. *J. Cryst. Growth,* vol. 270, pp. 184-191.